AD-A177 274 THE TURBULENT GRAVITY WAVE-CRITICAL LEVEL EVOLUTION OF ATMOSPHERIC FLOW..(U) GOULD OCEAN SYSTEMS DIV MIDDLETOWN RI HYDRONOMICS RESEARCH J R GRANT 19 DEC 86 GOULD-OSD-771-HYDRO-CR-86-10 1/1

UNCLASSIFIED F/G 4/1 NL

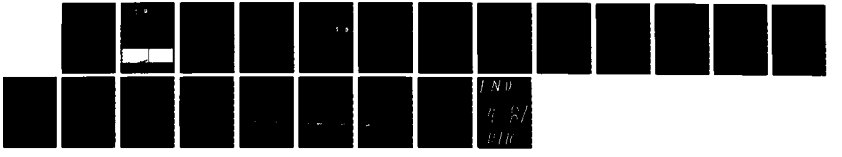

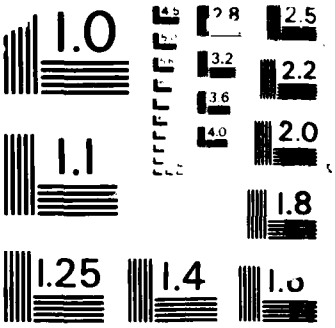

AFOSR-TR- 87-0102

**Approved for public release;
distribution unlimited.**

GOULD

HYDRODYNAMICS RESEARCH

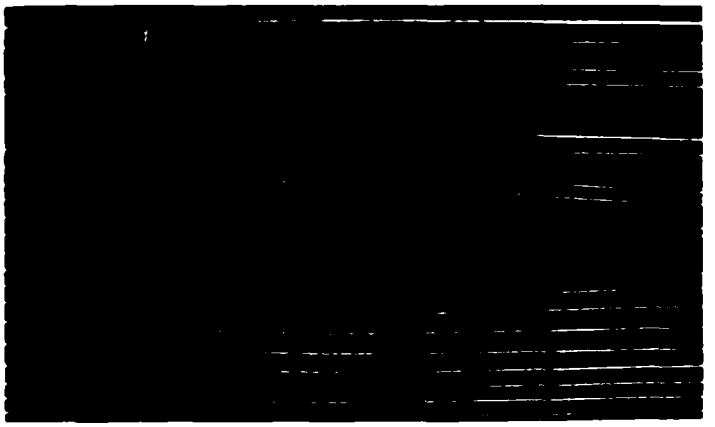

ASW SYSTEMS ENGINEERING FACILITY ● NEWPORT, RHODE ISLAND

Unclassified

SECURITY CLASSIFICATION OF THIS PAGE

AD-A187 274

REPORT DOCUMENTATION PAGE

1a. REPORT SECURITY CLASSIFICATION: UNCLASSIFIED	1b. RESTRICTIVE MARKINGS: NONE
2a. SECURITY CLASSIFICATION AUTHORITY: –	3. DISTRIBUTION/AVAILABILITY OF REPORT: Approved for public release Distribution unlimited
2b. DECLASSIFICATION/DOWNGRADING SCHEDULE: –	
4. PERFORMING ORGANIZATION REPORT NUMBER(S): GOULD-OSD-771-HYDRO-CR-86-10	5. MONITORING ORGANIZATION REPORT NUMBER(S): AFOSR-TR- 87-0102
6a. NAME OF PERFORMING ORGANIZATION: GOULD OCEAN SYSTEMS DIVISION; 6b. OFFICE SYMBOL (If applicable):	7a. NAME OF MONITORING ORGANIZATION: Air Force Office of Scientific Research/NC
6c. ADDRESS (City, State and ZIP Code): One Corporate Place/Newport Corporate Park Middletown, Rhode Island, 02840	7b. ADDRESS (City, State and ZIP Code): Bolling AFB Washington, DC 20332-6448
8a. NAME OF FUNDING/SPONSORING ORGANIZATION: AFOSR; 8b. OFFICE SYMBOL (If applicable): NC	9. PROCUREMENT INSTRUMENT IDENTIFICATION NUMBER: F49620-85-C-0114
8c. ADDRESS (City, State and ZIP Code): Bolling AFB Washington, DC 20332-6448	10. SOURCE OF FUNDING NOS. — PROGRAM ELEMENT NO.: 61102F; PROJECT NO.: 2310; TASK NO.: A1; WORK UNIT NO.:
The Turbulent Gravity-Wave Critical-Level Evolution of Atmospheric Flow (U)	
12. PERSONAL AUTHOR(S): J.R. Grant	
13a. TYPE OF REPORT: FINAL; 13b. TIME COVERED: FROM _____ TO _____	14. DATE OF REPORT (Yr., Mo., Day): 1986 December 19; 15. PAGE COUNT: 20
16. SUPPLEMENTARY NOTATION	
17. COSATI CODES — FIELD / GROUP / SUB. GR.	18. SUBJECT TERMS (Continue on reverse if necessary and identify by block number): Gravity Waves, Turbulence, Critical Level

19. ABSTRACT (Continue on reverse if necessary and identify by block number)

SEE REVERSE

20. DISTRIBUTION/AVAILABILITY OF ABSTRACT: UNCLASSIFIED/UNLIMITED ☒ SAME AS RPT. ☒ DTIC USERS ☐	21. ABSTRACT SECURITY CLASSIFICATION: Unclassified
22a. NAME OF RESPONSIBLE INDIVIDUAL: Lt Col James P. Koermer	22b. TELEPHONE NUMBER (Include Area Code): (202) 767-4960; 22c. OFFICE SYMBOL: NC

DD FORM 1473, 83 APR EDITION OF 1 JAN 73 IS OBSOLETE.

UNCLASSIFIED

SECURITY CLASSIFICATION OF THIS PAGE

19.

ABSTRACT

Strong turbulence may be produced when an internal gravity wave encounters a critical level. This turbulence can dissipate the wave motion, so that the momentum transported by the wave is deposited into the mean flow. Thus, gravity wave-critical level encounters are a significant mechanism by which the wind may be modified by gravity waves.

Such an encounter has been computed. The rms turbulent velocities are seen to be a substantial fraction (some 25%) of the wave-induced velocity. The absorption of the wave is seen to alter the wind profile, with turbulence distributing the wave momentum flux above and below the critical level. A variety of features of the wave and turbulence motion may be extracted. One which will be useful for comparison with radar observations is the refractive index structure function C_n^2, and contour plots are displaced.

Several other quantities depicting the evolution of the encounter also are presented. Plans for a detailed analysis of these and new computations are outlined. Also discussed are comparisons of these calculations with Doppler radar observations and laboratory measurements.

GOULD-OSD-771-HYDRO-CR-86-10
19 December 1986

THE TURBULENT GRAVITY-WAVE
CRITICAL-LEVEL EVOLUTION OF ATMOSPHERIC FLOW

A REPORT FOR 1986

submitted to:

Lt. Col. James P. Koermer, Program Manager
Directorate of Chemical and Atmospheric Sciences
Air Force Office of Scientific Research
Bolling AFB
Washington, DC 20322

by

John R. Grant, Ph.D.

Gould Defense Systems, Inc.
Ocean Systems Division
One Corporate Place
Newport Corporate Park
Middletown, Rhode Island 02840

TABLE OF CONTENTS

ABSTRACT

Strong turbulence may be produced when an internal gravity wave encounters a critical level. This turbulence can dissipate the wave motion, so that the momentum transported by the wave is deposited into the mean flow. Thus, gravity wave-critical level encounters are a significant mechanism by which the wind may be modified by gravity waves.

Such an encounter has been computed. The rms turbulent velocities are seen to be a substantial fraction (some 25%) of the wave-induced velocity. The absorption of the wave is seen to alter the wind profile, with turbulence distributing the wave momentum flux above and below the critical level. A variety of features of the wave and turbulence motion may be extracted. One which will be useful for comparison with radar observations is the refractive index structure function C_n^2, and contour plots are displaced.

Several other quantities depicting the evolution of the encounter also are presented. Plans for a detailed analysis of these and new computations are outlined. Also discussed are comparisons of these calculations with Doppler radar observations and laboratory measurements.

INTRODUCTION

The specific purpose of this work is to study numerically the turbulent gravity-wave critical-level encounter. The larger context of the study is the manner in which gravity waves alter the mean wind. As will be seen in results presented below, this encounter can be a site of strong turbulence production by wave breaking as the wave approaches the critical level (where the wind speed in the direction of wave propagation matches the wave phase speed). This turbulence dissipates the wave motion, so that momentum transferred by the wave is deposited into the mean flow.

A second important point of the work is the investigation of the characteristics of the generated turbulence. Many features of the turbulence field emerge from the calculations; one of the most interesting is the computation of the refractive index structure function C_n^2. This quantity may be deduced from the strength of radar backscatter and so is a natural and useful point of convergence between the numerical calculations and radar observations of the atmosphere. These results are, to my knowledge, the first calculations of their kind.

The gravity-wave critical level encounter produces strong dynamical forces and rapid transfer of energy among the wave spectral components, a reflection of its well-known vigorous nature. Because of this vigor, the numerical calculations have been found to be rather difficult when turbulence is also allowed to develop. However, an emphasis on very stable marching algorithms has enabled a calculation to be carried out. These computations are the particular important achievement of the work for the past year. Now a detailed investigation of the encounter may be made using these and new calculations.

The next section highlights these results, and a concluding section outlines the course of the study for the next year. An appendix displays the mathematical equations which are solved numerically.

NUMERICAL CALCULATIONS

In order to minimize ambiguity in interpreting the results, the computation has been arranged to model an ideal case; however, the values assigned to scales and parameters are certainly commonly realized in the atmosphere, e.g., a wave encounter with a shear layer associated with the polar jet stream.

The wind is described by the frequently used hyperbolic tangent profile

$$u(z) = U\,[\tanh(z/H) + 1],$$

and the potential temperature is exponentially increasing with height z so that the Brunt-Vaisala frequency is constant:

$$N(z) = N.$$

The values assigned to the velocity and height scales are

$$U = 14.142 \text{ meters/sec}$$
$$H = 1000 \text{ meters}$$

and

$$N = 0.0112 \text{ rad/sec}.$$

Hence the minimum Richardson number is

$$Ri_{min} = (NH/U)^2 = 2.$$

A plot of the wind profile is shown in Figure 1. The height range shown is that of the calculation:

$$-4 \leq z/H \leq 2.$$

In this figure and all following figures, all quantities are non-dimensionalized by U and H. The exception is C_n^2, which is given dimensionally (i.e., in meters$^{-2/3}$).

The wave is forced at the bottom of the computational domain by a boundary condition equivalent to the requirement on the wave-induced vertical velocity component w that

$$w(x,z,t) = F(t)\ W \sin(kx - \omega t),\ z/H = -4,$$

where

$$W/U = 0.1$$
$$kH = 0.5$$
$$\omega H/U = 0.5.$$

The amplitude function is

$$F(t) = \sin^2(\pi\, t/T)$$

with

$$T = 3 \text{ wave periods.}$$

Hence the wave emerges with initially small but increasingly larger amplitude (avoiding startup transients), and after three periods propagates away from the bottom boundary without being re-generated there. About one wave period is generated with substantial amplitude. Although the generation amplitude W is not small, neither is it unusually large; that is, the dramatic evolution of the wave as it approaches the critical level is not due to a synthetically enormous wave amplitude, but, rather, to the fluid dynamics associated with such encounters.

Note the wave parameters are chosen so that the critical level is at $z = 0$:

$$u(z)/U = (\omega H/U)/(kH) \quad \text{at} \quad z = 0.$$

The positive-definite turbulence correlations are set to the value 10^{-7}, which essentially is zero. The correlations (e.g., momentum flux) are set exactly to zero.

The number of grid-points in the z direction is 151, and there are 24 spectral modes, or, with the Fast Fourier Transform conventions, 48 points in the horizontal. The calculation extends to 4.25 periods, with a time step size of 0.01 periods.

An overview of the evolution of the encounter is obtained from Figure 2. Plotted there are the minimum value of the total (mean plus wave) potential temperature gradient, maximum turbulent variance in the horizontal velocity component, and maximum turbulent heat flux. The potential temperature gradient initially decreases from 2 due to emergence of the wave at the lower boundary; the wave amplitude there is not sufficient -- even at the maximum at t = 1.5 periods -- to drive this gradient negative. However, as the wave encounters the critical level, there the larger Lagrangian displacements of fluid results in denser air being pulled up over less dense; this is indicated by the temperature gradient becoming negative. About one-half wave period later the instability of this arrangement produces a turbulent heat flux which almost immediately leads to rapid generation of turbulent velocity fluctuations. The amplitude of the variance shown in Figure 2 is about 0.06, corresponding to a rms value of about 0.25. Since the (nondimensional) horizontal wave-induced velocity maximum is about 1.0, we see that the turbulent velocity fluctuations are quite significant compared to the wave velocities. As the turbulence restores the stable stratification, its source of energy is correspondingly diminished, and eventually the turbulent motions die away under the combined influence of dissipation, diffusion, and stratification.

This encounter is more vividly depicted by plots in the x - z (i.e., computational) plane. Accordingly, contour plots of potential temperature, turbulent kinetic energy, and C_n^2, and vector plots of the wave-induced velocity are shown at time 1.5, 3.0, 3.5, and 4.25 periods in Figures 3, 4, 5, and 6, respectively. In these plots, the z coordinate again ranges over $-4 \leq z/H \leq 2$, and the x coordinate ranges over on wavelength = 4π.

In Figure 3, the upper edge of the wave is just reaching the critical level at z = 0. Most of the wave is still in the region of little shear, the wave phase lines are nearly straight, and the displacements revealed by the shape of the potential temperature contours are approximately sinusoidal (linear). No turbulence has been generated.

In Figure 4, at 3.0 periods, the wave is well into its encounter with the critical level. Just below this level, the potential temperature contours display the pronounced 'overhang' of denser air over less dense air. The vector plot shows that the wave is just beginning to plunge downward, driven by the buoyancy forces associated with this overhang. This unstable stratification also has resulted in an almost explosive growth of turbulence; note the coincidence of the turbulent kinetic energy with the region of unstable stratification. There has been some discussion in the literature about whether these encounters will generate turbulence by this sort of convective instability, or if the mechanism is through shear (or 'dynamic') production. This result unequivocally indicates that it is the former case for waves of this period and wavelength. The contour plot of C_n^2 shows that it generally follows the gross features displayed by the contour plot of turbulent kinetic energy, as may be expected. The value of mean density used in computing C_n^2 is a tropopause value of 0.42 kg/m. The peak of C_n^2 in this plot is about 10^{-14} meters $^{-2/3}$, which is roughly two orders of magnitude greater than that observed by Doppler radar during wave events at this altitude. However, the geometrical extent of the peak values is rather small, much less than a radar beamwidth, so the calculations seem satisfactory.

By 3.5 periods (Figure 5) the downward plunge of the wave has taken place and energy has cascaded to higher spectral modes, as seen from the vector plot given in this figure. These higher modes are evanescent, not propagating away. Much of the original, identifiable structure of the wave has been destroyed. The relatively strong stable stratification so created inhibits the downward diffusion of the turbulent kinetic energy and results in a concentration of the refractive index fluctuations (as indicated by the contour plot of C_n^2) near the bottom of the region of turbulent activity. These features are qualitatively similar to those seen in photographs of laboratory gravity-wave critical level encounters. Remnants of the wave motion advect the turbulence upward into levels of greater wind speed (e.g., near z = 0), and this process is aided by upward diffusion. The greater wind then advects the turbulence horizontally, stretching it out nearly across the entire wavelength.

Figure 6 displays the situation at 4.25 periods. Little of the form of the original wave motion remains; the wave motion is dominated by the 'sloshing' of the shorter wavelength evanescent modes. Notice that in the region of remaining turbulent activity there is little wave motion, it

having been damped out by the turbulence. The turbulence, under the influence of stable instead of unstable stratification, is rapidly dying away. The different advection rates by wind at differing levels has formed the remaining turbulence into a fairly thin quasi-homogeneous layer.

Finally, the wind profile at this last time of 4.25 periods is shown in Figure 7. Even though the wave was generated with substantial amplitude for only about one period, the significant increase in wind speed around the critical level is evident.

RESEARCH PLANS FOR THE COMING YEAR

In the context of modification of the wind, a central point of inquiry is the behavior of the momentum transport by the wave motion and the turbulence as the critical level encounter proceeds. Accordingly, a focus of the upcoming work will be on this transport, as revealed by the calculations, in particular, on how the momentum transport is shared between the wave motion and the turbulence, and how it is distributed over the mean flow as the wave is absorbed. Further, the heat flux plays a major role in the critical level encounter, as may be seen in the results presented above. Thus, this transport also will be an important subject of the study. There have been in recent years several speculations in the literature on the relative magnitude of the momentum and heat transports in wave breaking events, usually cast in terms of the question as to the magnitude of the Prandtl number. The calculations presented above and those to be performed allow an immediate and direct computation of the magnitudes in question.

These mean momentum and heat fluxes mediate the modification of the mean wind and temperature profiles by the breaking wave. The fluctuating components of these fluxes modify and dissipate the wave itself. This direct interaction between the wave motion and the turbulence is an important feature in its own right, and will be an important point of investigation in the upcoming study.

The new calculations will include cases where the wave is forced for more than the approximately one wave period of the case shown above. Such longer wave-train cases are more typical of atmospheric waves.

Plots of C_n^2 such as those given above will be made for all cases computed. Radar records in which suitably monochromatic wave events have been identified will be compared to these calculated results. The Poker Flat, Alaska and the Sunset Colorado Doppler radars appear to be the best candidate instruments for such comparison. Even order-of-magnitude agreement will lend confidence in the atmospheric relevance of these calculations.

Finally, the six-foot diameter annular tank constructed and operated at Northwest Research Associates (formerly Physical Dynamics, Inc.) may provide measurements of breaking waves which will enable fairly detailed comparison with results of these numerical calculations. Such comparison would both test the numerics as well as provide insight into the breaking wave observations.

APPENDIX: MATHEMATICAL FORMULATION

$$\frac{\partial \langle u_i' u_j' \rangle}{\partial t} = J(\langle u_i' u_j' \rangle, \langle \psi \rangle) + \partial_k \left(c_q \frac{q}{\varepsilon} \langle u_k' u_l' \rangle \partial_l \langle u_i' u_j' \rangle \right)$$

$$+ P_{ij} + G_{ij} + \phi_{ij} - \frac{2}{3} \delta_{ij} \varepsilon$$

$$q \equiv \frac{1}{2} \langle u_i' u_i' \rangle$$

$$P_{ij} \equiv -\langle u_i' u_k' \rangle \partial_k \langle u_j \rangle - \langle u_j' u_k' \rangle \partial_k \langle u_i \rangle$$

$$G_{ij} \equiv \beta_i \langle \theta' u_j' \rangle + \beta_j \langle \theta' u_i' \rangle$$

$$\phi_{ij} \equiv \phi_{ij1} + \phi_{ij2} + \phi_{ij3}$$

$$\phi_{ij1} \equiv -c_1 \frac{\varepsilon}{q} \left(\langle u_i' u_j' \rangle - \frac{2}{3} \delta_{ij} q \right)$$

$$\phi_{ij2} \equiv -c_2 \left(P_{ij} - \frac{2}{3} \delta_{ij} P \right), \quad P \equiv \frac{1}{2} P_{ii}$$

$$\phi_{ij3} \equiv -c_3 \left(G_{ij} - \frac{2}{3} \delta_{ij} G \right), \quad G \equiv \frac{1}{2} G_{ii}$$

$$\frac{\partial \varepsilon}{\partial t} = J(\varepsilon, \langle \psi \rangle) + \partial_k \left(c_\varepsilon \frac{q}{\varepsilon} \langle u_k' u_l' \rangle \partial_l \varepsilon \right)$$

$$+ \frac{\varepsilon}{q} \left(c_{\varepsilon 1} P + c_{\varepsilon 1} G \right) - c_{\varepsilon 2} \varepsilon^2 / q$$

$$\frac{\partial \langle\theta\, u_i'\rangle}{\partial t} = J(\langle\theta' u_i'\rangle, \langle\psi\rangle) + \partial_k \left(c_{q\theta} \langle u_k' u_i'\rangle \frac{q}{\varepsilon} \partial_l \langle\theta' u_l'\rangle\right)$$

$$+ P_{\theta i1} + P_{\theta i2} + G_{\theta i} + \phi_{\theta i}$$

$$P_{\theta i1} \equiv \langle u_i' u_k'\rangle \partial_k \langle\theta\rangle$$

$$P_{\theta i2} \equiv -\langle\theta' u_k'\rangle \partial_k \langle u_i\rangle$$

$$G_i \equiv \beta_i \langle\theta'^2\rangle$$

$$\phi_{\theta i} \equiv \phi_{\theta i1} + \phi_{\theta i2} + \phi_{\theta i3}$$

$$\phi_{\theta i1} \equiv -c_{\theta 1} \frac{\varepsilon}{q} \langle\theta' u_i'\rangle$$

$$\phi_{\theta i2} \equiv -c_{\theta 2} P_{\theta i2}$$

$$\phi_{\theta i3} \equiv -c_{\theta 3} P_{\theta i3}$$

$$\frac{\partial \langle\theta'^2\rangle}{\partial t} = J(\langle\theta'^2\rangle, \langle\psi\rangle) + \partial_k \left(c_q \langle u_k' u_l'\rangle \frac{q}{\varepsilon} \partial_l \langle\theta'^2\rangle\right)$$

$$- 2\langle\theta' u_l'\rangle \partial_l \langle\theta\rangle - c_\theta (\langle\theta'^2\rangle/q)\, \varepsilon$$

$$\frac{\partial \langle\theta\rangle}{\partial t} = J(\langle\theta\rangle, \langle\psi\rangle) + \frac{\nu}{P} \nabla^2 \langle\theta\rangle - \partial_l \langle\theta' u_l'\rangle$$

$$\frac{\partial \langle\zeta\rangle}{\partial t} = J(\langle\zeta\rangle, \langle\psi\rangle) + \nu \nabla^2 \langle\zeta\rangle - \beta\, \partial \langle\theta\rangle/\partial x$$

$$- (\partial_3^2 - \partial_1^2) \langle u_1' u_3'\rangle - \partial_1 \partial_3 (\langle u'^2\rangle - \langle w'^2\rangle)$$

$$(\partial_1^2 + \partial_3^2) \langle\psi\rangle = -\langle\zeta\rangle$$

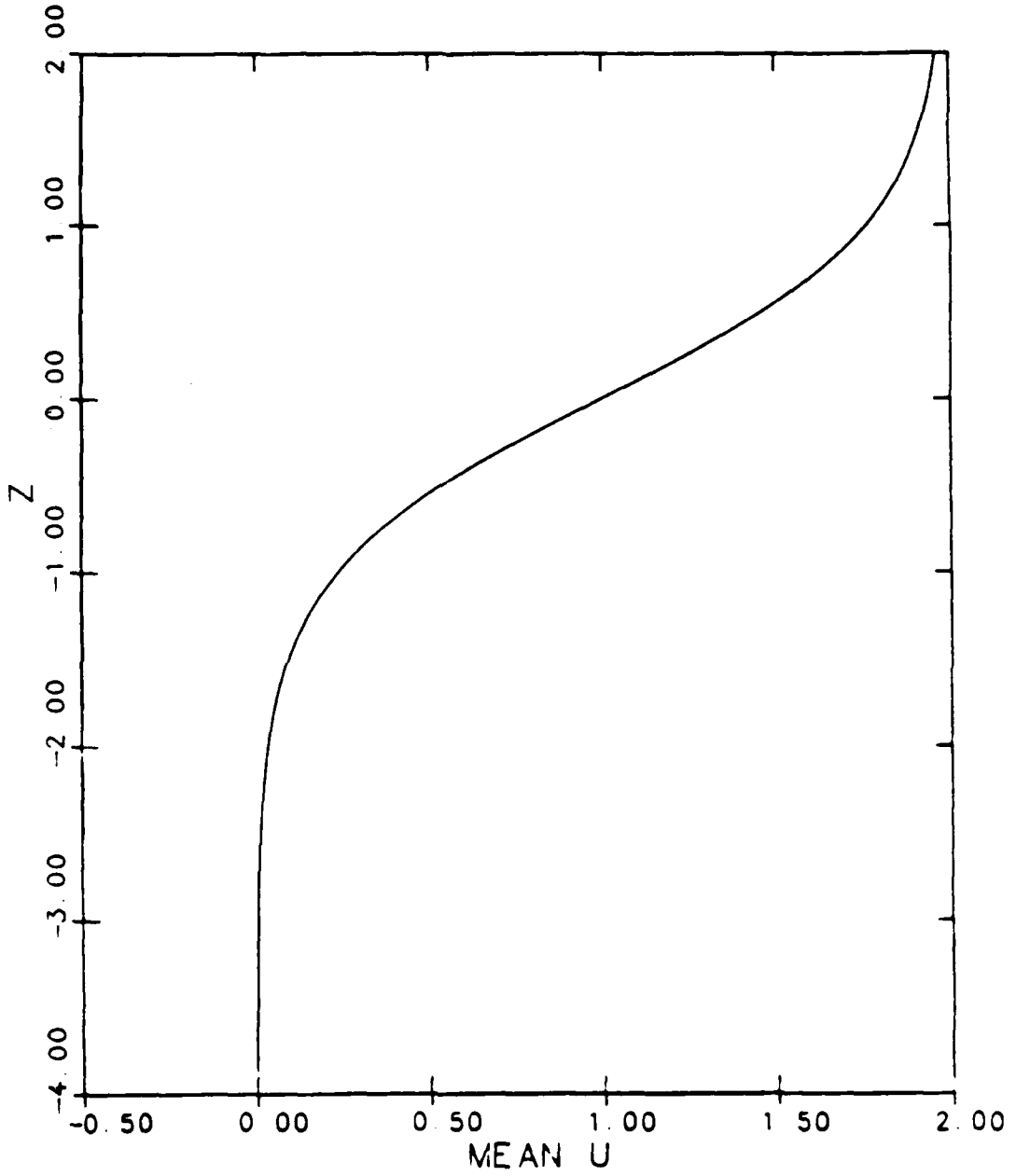

Figure 1. INITIAL WIND PROFILE.

JRG/sg/2419m

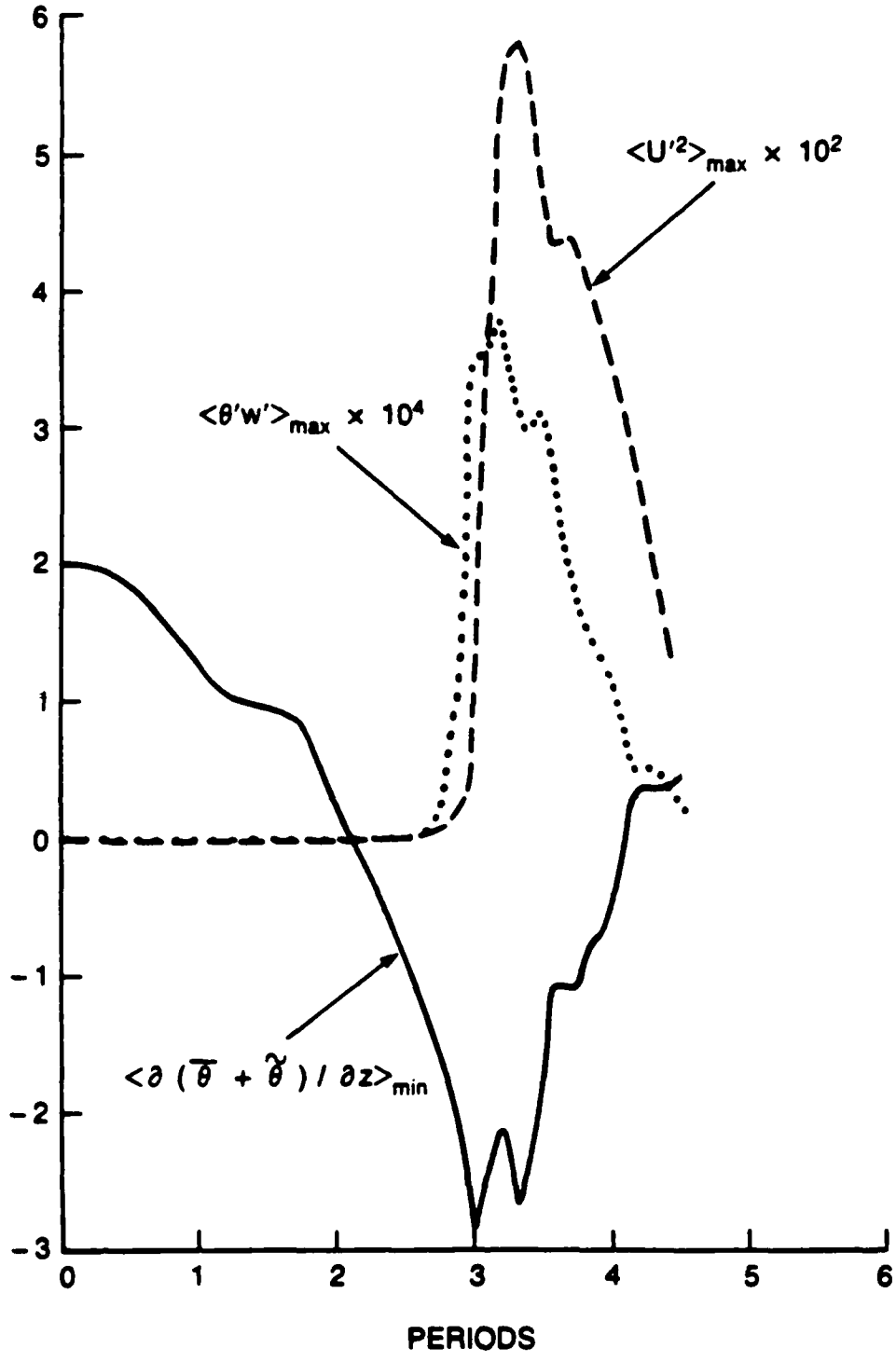

863140834-5

Figure 2. EVOLUTION OF MINIMUM POTENTIAL TEMPERATURE GRADIENT, MAXIMUM HEAT FLUX, AND MAXIMUM VARIANCE IN HORIZONTAL VELOCITY.

JRG/sg/2419m

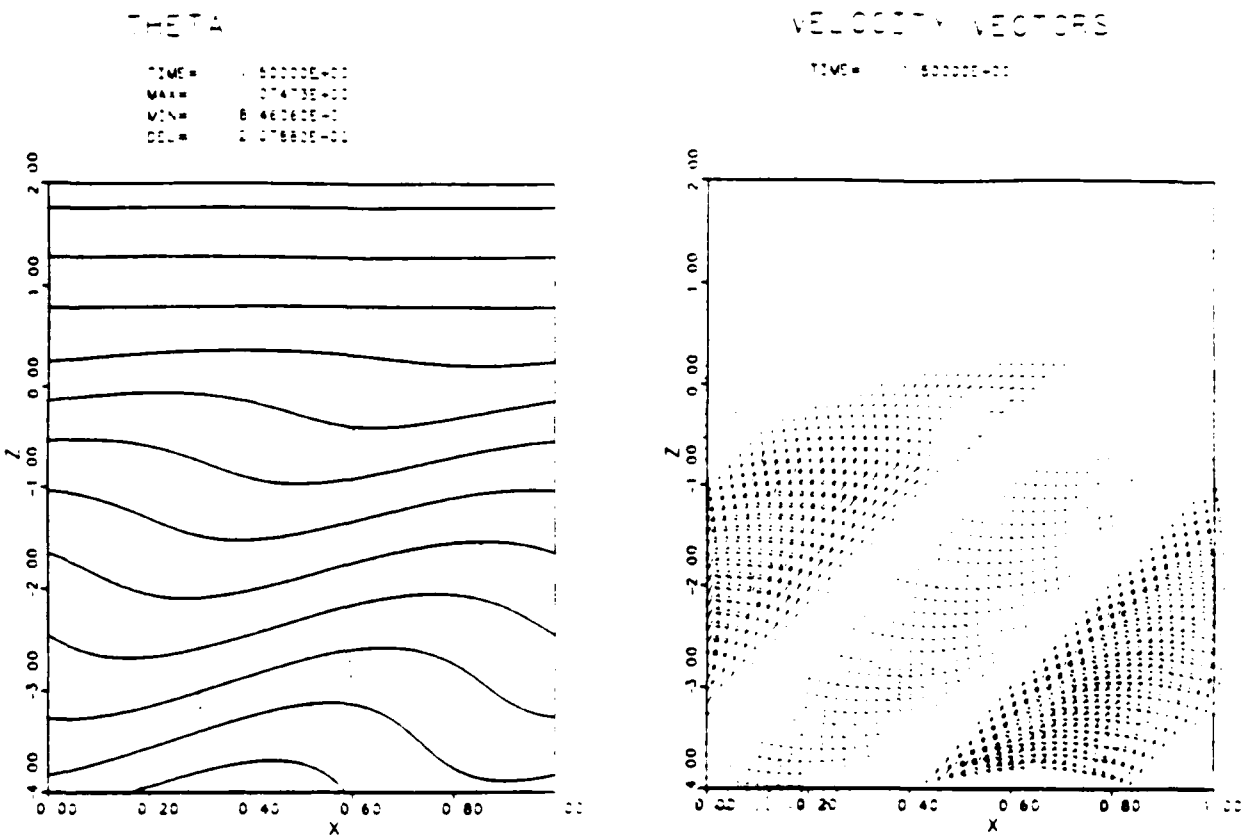

Figure 3. AT t = 1.5 PERIODS, CONTOUR PLOT OF POTENTIAL TEMPERATURE AND A VELOCITY VECTOR PLOT.

JRG/sg/2419m

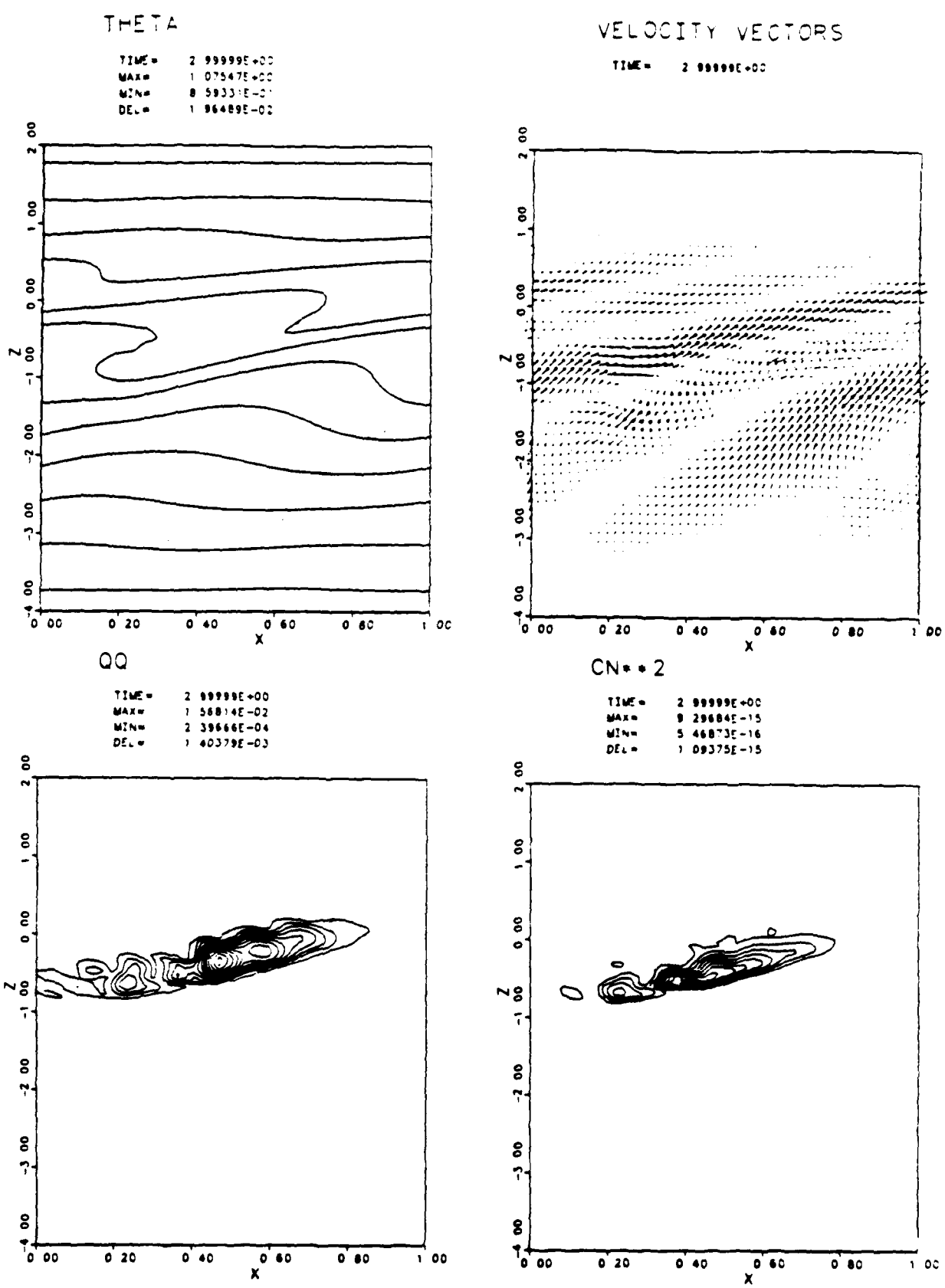

Figure 4. AT t = 3.0 PERIODS, CONTOUR PLOTS OF POTENTIAL TEMPERATURE, TURBULENT KINETIC ENERGY, AND C_n^2, AND A VELOCITY VECTOR PLOT.

JRG/sg/2419m

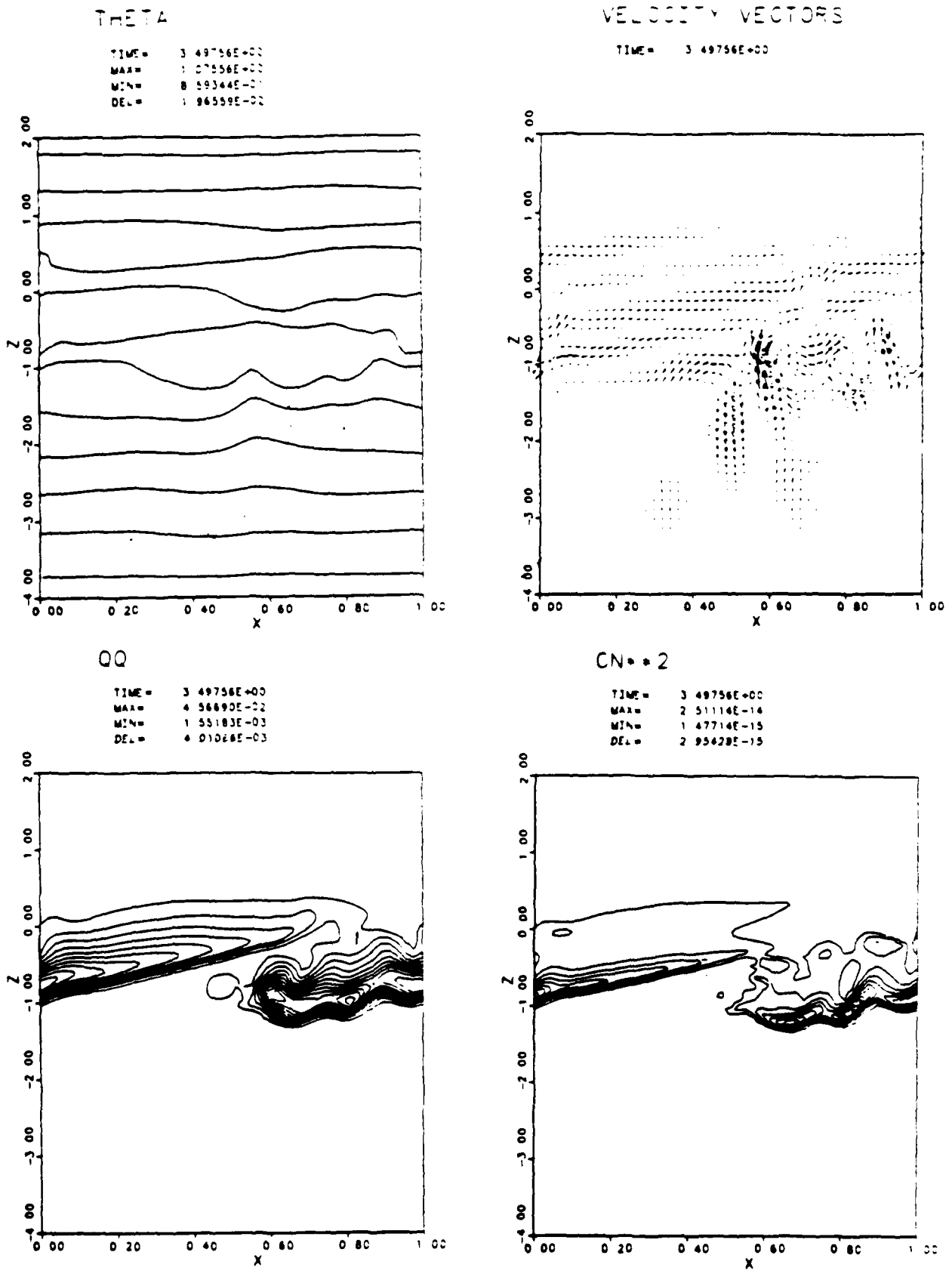

Figure 5. AT t = 3.0 PERIODS, CONTOUR PLOTS OF POTENTIAL TEMPERATURE, TURBULENT KINETIC ENERGY, AND C_n^2, AND A VELOCITY VECTOR PLOT.

JRG/sg/2419m

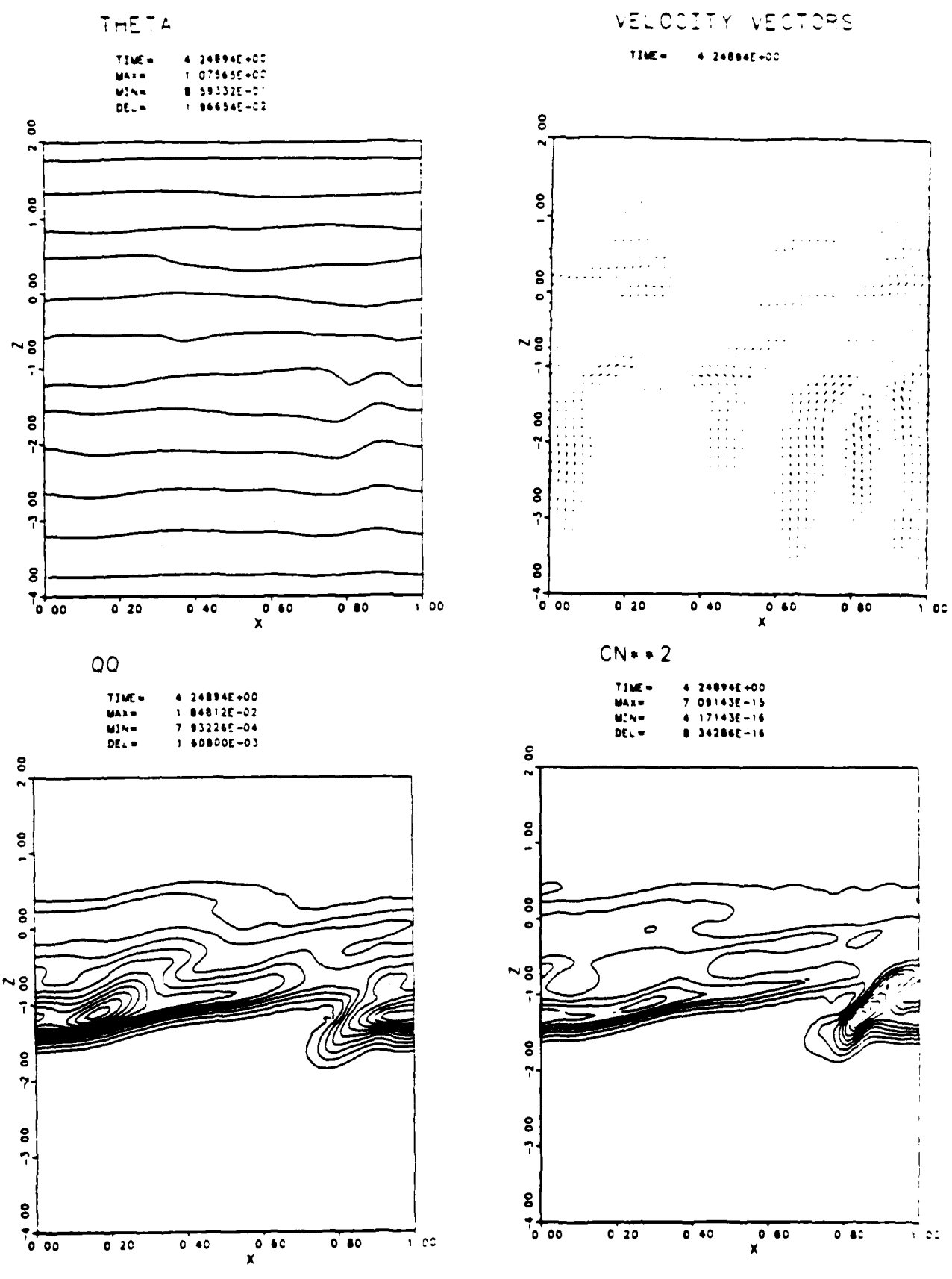

Figure 6. AT t = 3.0 PERIODS, CONTOUR PLOTS OF POTENTIAL TEMPERATURE, TURBULENT KINETIC ENERGY, AND C_n^2, AND A VELOCITY VECTOR PLOT.

JRG/sg/2419m

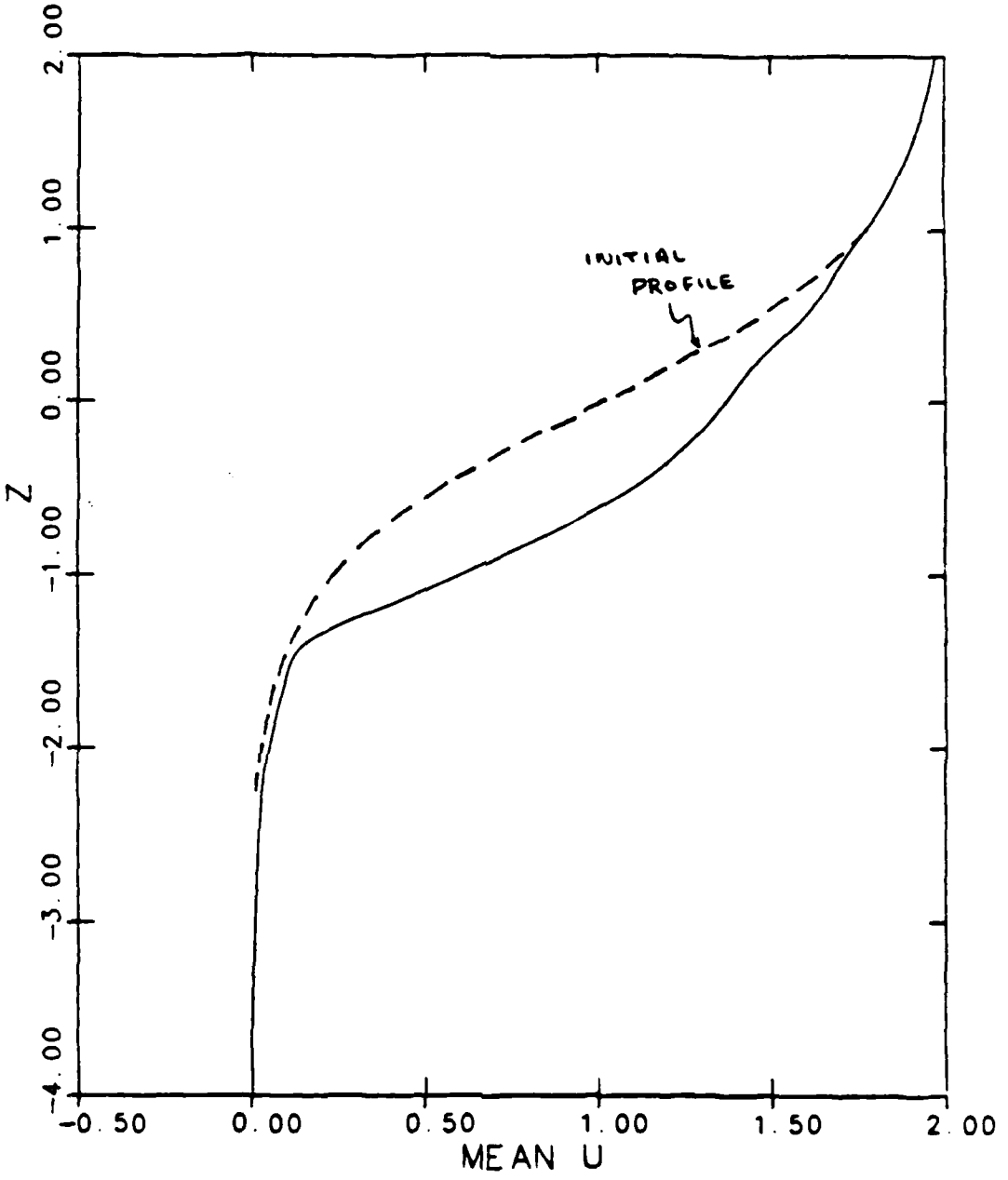

Figure 7. WIND PROFILE AT t = 4.25 PERIODS.

JRG/sg/2419m

END

4-87

DTIC